Exp Fluids (2008) 44:851–863
DOI 10.1007/s00348-008-0496-2

REVIEW ARTICLE

Planar laser induced fluorescence in aqueous flows

J. P. Crimaldi

Received: 14 November 2007 / Revised: 17 March 2008 / Accepted: 18 March 2008 / Published online: 4 April 2008

Abstract Planar laser-induced fluorescence (PLIF) is a non-intrusive technique for measuring scalar concentrations in fluid flows. A fluorescent dye is used as a scalar proxy, and local fluorescence caused by excitation from a thin laser sheet can be related to dye concentration. This review covers quantitative PLIF in aqueous flows, with discussions of fluorescence theory, experimental methods and equipment, image processing and calibration, and applications of the technique.

1 Introduction

The use of soluble dyes for aqueous flow visualization was already in evidence in the nineteenth century, when Osbourne Reynolds performed his famous experiments on laminar and turbulent flow in round pipes (Reynolds 1883). However, a quantitative extension to this visualization technique would not appear for another century, when laser-induced fluorescence (LIF) was pioneered by Dewey (1976), Owen (1976), and Liu et al. (1977). The technique was then adopted in earnest by Paul Dimotakis at Caltech who, along with his students Manoochehr Koochesfahani and Werner Dahm, published a number of early seminal LIF studies (e.g., Dimotakis et al. 1983; Koochesfahani and Dimotakis 1986; Dahm and Dimotakis 1987). Two excellent early tutorials on the topic are given by Walker (1987) and Ferrier et al. (1993). LIF can be used to measure scalar concentrations at a point (e.g., Sreenivasan and Prasad 1989; Komori et al. 1993), along a line (e.g., Koochesfahani and Dimotakis 1985; Hannoun and List 1988; Papantoniou and List 1989), in two-dimensional planes (Dahm and Dimotakis 1987), and in three-dimensional volumes (e.g., Tian and Roberts 2003; Van Vliet et al. 2004).

The most common application of LIF in fluid flows is two-dimensional planar laser-induced fluorescence (PLIF). The focus of this review article is on the quantitative application of PLIF to aqueous flows (for PLIF in gaseous flows, see Van Cruyningen et al. 1990). While three-dimensional LIF methodology is not extensively discussed in this review, the methodology is a simple extension of the two-dimensional techniques.

In all forms of LIF, a laser is used to excite a fluorescent species within the flow. Typically, the tracer is an organic fluorescent dye such as fluorescein or rhodamine. The dye absorbs a portion of the excitation energy and spontaneously re-emits a portion of the absorbed energy as fluorescence. The fluorescence is measured optically and used to infer the local concentration of the dye.

2 Theoretical background

2.1 General fluorescence theory

The general relationship between local fluorescence F, local excitation intensity I, and local concentration C has the form

$$F \propto \frac{I}{1 + I/I_{\text{sat}}} C \tag{1}$$

where I_{sat} is the saturation intensity for the dye. Fluorescence saturation occurs when the rate of excitation

J. P. Crimaldi (✉)
Department of Civil and Environmental Engineering,
University of Colorado, Boulder, CO 80309-0428, USA
e-mail: crimaldi@colorado.edu

exceeds the fluorophore deactivation rate (e.g., Patsayeva et al. 1999), leading to the non-linear relationship between F and I. However, if $I \ll I_{sat}$, the excitation is called "weak", and Eq. 1 is linearized to the form

$$F \propto IC \tag{2}$$

Unless otherwise noted, weak excitation (and thus the validity of Eq. 2) is assumed throughout this review. As detailed in Sect. 3.2, high dye concentrations can produce non-linearities in fluorescence due to absorption-related changes in the local value of I, but Eq. 2 nonetheless remains valid.

In principle, Eq. 2 provides a simple method for experimental determination of local concentrations through measurement of F. However, the local excitation intensity I is typically unknown, is not independently measured, and can vary spatially and temporally according to the instantaneous concentrations along the ray path. According to the Beer–Lambert law, absorption causes a ray of light with intensity I passing an infinitesimal distance dr through a solution with dye concentration C to experience an intensity change

$$\frac{\mathrm{d}I}{I} = -\epsilon\, C\, \mathrm{d}r \tag{3}$$

where ε is an absorption (or extinction) coefficient (Walker 1987). The local intensity of a ray passing from $r = r_0$ to $r = r_1$ through a spatially variable concentration field is thus

$$I(r_1) = I(r_0) \exp\left[-\epsilon \int_{r_0}^{r_1} C(r)\mathrm{d}r\right] \tag{4}$$

Attenuation along a path from r_0 to r_1 is negligible if

$$\epsilon \int_{r_1}^{r_2} C(r)\mathrm{d}r \ll 1 \tag{5}$$

For a uniform concentration field, this inequality reduces to $\varepsilon bC \ll 1$, where $b = r_1 - r_0$. Systems with path lengths and concentrations that satisfy Eq. 5 are called "optically thin" (Melton and Lipp 2003).

A fraction of the light energy absorbed locally by the dye is subsequently emitted as fluorescence in the emission band. The ratio of light energy emitted to that absorbed is called the quantum efficiency, ϕ. Consider an infinitesimal right prismatic volume oriented along the axis of the incident excitation ray, with a volume $\mathrm{d}V = \mathrm{d}r\ \mathrm{d}A$, where d$r$ is the length of the prism in the ray direction, and dA is the cross-sectional area normal to the ray. A uniform dye concentration C within the volume illuminated by a local excitation intensity I fluoresces omnidirectionally with power

$$\mathrm{d}F = -\phi\ \mathrm{d}I\ \mathrm{d}A \tag{6}$$

Equations 3 and 6 combine to give

$$\mathrm{d}F = \phi\ \epsilon I\ C\ \mathrm{d}V \tag{7}$$

which is a formal statement of Eq. 2 along a ray path, with I given by Eq. 4.

2.2 Theory as applied to PLIF

For most PLIF applications, a radial laser sheet is formed by a narrow beam passing through sheet optics located at the origin (Fig. 1). At radial distances that are large compared to the incoming beam diameter, the sheet will have an intensity distribution of the general form

$$I(r, \theta, z) = P\ a(r, \theta) f(r) g(\theta) h(z) \tag{8}$$

where P is the power in the incoming beam, and $a(r,\theta)$ is the dimensionless attenuation along ray paths due to dye absorption, which, from Eq. 4, is

$$a(r, \theta) = \exp\left[-\epsilon \int_0^r C(r', \theta)\mathrm{d}r'\right] \tag{9}$$

The unattenuated spatial intensity distribution of the sheet is $f(r)g(\theta)h(z)$. For the radial sheet shown in Fig. 1, $f(r) = r^{-1}$. The functions $g(\theta)$ and $h(z)$ depend on the shape of the original beam and the nature of the sheet-forming optics, and are defined such that they each integrate to unity over the entire θ and z ranges of the sheet, respectively.

Typically, the flow is imaged from a camera placed normal to the laser sheet. Consider a small area $\Delta A = r\Delta r\Delta\theta$ in the plane of the sheet. The camera will image fluorescence from a right prismatic volume ΔV

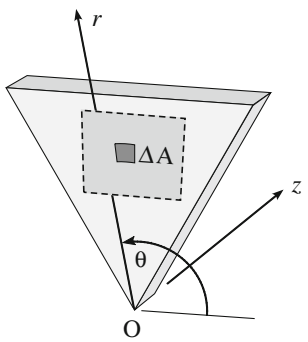

Fig. 1 Schematic of a radial laser sheet showing the coordinate system used in the text. Optics that form the sheet are located at the origin "O". The *dashed rectangle* is the region to be imaged by the camera, and the *smaller shaded area* is the area ΔA in Eqs. 10 and 11

formed by projecting ΔA across the width of the sheet (i.e., the entire extent of $h(z)$). Integrating Eqs. (7) and (8) over this volume gives the total fluorescence

$$F = \phi \epsilon P \, a(r,\theta) f(r) g(\theta) C \Delta A \tag{10}$$

where it is understood that C is now the concentration averaged over the small imaged volume ΔV, with the average weighted in the z direction by $h(z)$. Assuming that any reabsorption of fluoresced light by dye along the receiving path (Lemoine et al. 1996) is negligible, the fluorescence intensity imaged at any camera pixel location (i, j) corresponding to coordinate (r, θ) is thus

$$I_F(i,j) = \beta(i,j)\frac{F}{\Delta A} = \alpha(i,j) a(r,\theta) C \tag{11}$$

where $\beta(i, j)$ is the fraction of the total omnidirectional fluorescence received by the camera optics at a particular pixel location, and $\alpha(i, j)$ is the collection of concentration-independent constants (with dimensions of intensity per concentration)

$$\alpha(i,j) = \beta(i,j)\phi\epsilon P f(r) g(\theta) \tag{12}$$

This permits an expression for determining C from measured values of I_F to be written as

$$C = [\alpha(i,j) a(r,\theta)]^{-1} I_F \tag{13}$$

where $a(r, \theta)$ can be numerically integrated for each individual image according to the instantaneous concentration field, and $\alpha(i, j)$ can be empirically determined, as discussed in Sect. 4. Following Koochesfahani and Dimotakis (1985), Eqs. (9) and (13) can be discretized along any ray $\theta = \theta_0$, yielding

$$C(k,\theta_0) \approx [\alpha(r,\theta_0)]^{-1} I_F \prod_{n=1}^{k-1} \exp[\epsilon C(n,\theta_0)\Delta r] \tag{14}$$

where the product of the exponentials results from the exponential of the sum in Eq. 9. This operation can be inconvenient for PLIF applications with radial laser sheets, since the polar integration along a ray path typically relies on data from a cartesian image. For this reason, $a(r, \theta)$ is often enforced to be very close to unity, through some combination of short ray path lengths and/or low concentrations. Alternatively, radial beam paths can be rendered parallel in the image region by passing the incident beam through a large confocal lens (e.g., Ferrier et al. 1993; Van Vliet et al. 2004).

If the concentration is uniform along the ray path, then Eqs. 4 and 7 reduce to

$$F(r_1) = I(r_0)\phi\epsilon C \exp(-\epsilon r C) \tag{15}$$

These relations permit experimental determination of ε for a given dye (e.g., Walker 1987; Ferrier et al. 1993).

3 Experimental configurations

3.1 Lasers

A PLIF system requires an appropriately paired laser and fluorescent dye combination, with at least part of the laser power within the absorption band of the dye. Continuous wave (CW) argon-ion lasers operating at 488 and/or 514.5 nm are used as the excitation source in approximately three-quarters of aqueous PLIF experiments reported in the fluid mechanics literature. Pulsed, frequency-doubled Nd:YAG lasers operating at 532 nm are used in most of the remaining experiments, and their use has become increasingly common in recent years. A few experiments have employed copper vapor lasers (Yoda et al. 1994; Karasso and Mungal 1996, 1997), and excimer lasers are sometimes used to initialize photoactivatable ("caged") dyes, but not for the excitation itself (Guilkey et al. 1996; Hansen et al. 2000; Koochesfahani et al. 2000).

Ion lasers have the advantage of having superior beam quality and a continuous output that facilitates flow visualization. When operated in the TEM00 mode, ion lasers output a beam that is reasonably close to a Gaussian cross-section, and when operated in a closed-loop light-regulated mode, have a stable power output that simplifies calibration of the PLIF system. By comparison, Nd:YAG lasers have inferior beam quality, and the power and distribution of the beam can vary from pulse to pulse (Law and Wang 2000). The main advantage of Nd:YAG lasers is their high power output, typically on the order of 10^7 W during the pulse, as opposed to a continuous output of 10 W or less for an ion laser. Even though the pulse length of the Nd:YAG is only on the order of 10 ns, the energy per image exposure is typically much higher than that obtainable with an ion laser, since the exposure time in the latter case is limited by relevant timescales in the flow (Karasso and Mungal 1997).

Ironically, the high power of the Nd:YAG lasers can be problematic. If the laser excitation intensity is not small relative to the saturation intensity of the dye, the weak excitation assumption (Sect. 2.1) is violated, resulting in a non-linear relationship between F and I. This effect can be significant with pulsed lasers, since short pulse times can lead to exceptionally high intensities, even as compared to those produced by high-power CW lasers. A CW laser operating in the optimal TEM00 mode has a peak centerline intensity of $8P/\pi d^2$, where d is the beam diameter measured to the e^{-2} intensity contour. A typical light sheet formed by scanning a CW beam with a mirror has local peak intensities of order 10^7 W/m^2 (e.g., Troy and Koseff 2005a), with intensities several orders of magnitude lower if a continuous sheet is formed by spreading the laser through a cylindrical lens. A typical light sheet formed

with a pulsed Nd:YAG laser has intensities of order 10^{11} W/m^2 (e.g., Karasso and Mungal 1996; Shan et al. 2004). Values of I_{sat} have been estimated or inferred for both Rhodamine 6G (Shan et al. 2004) and Rhomdamine WT (Melton and Lipp 2003) to be of order 10^{10} W/m^2, which is significantly above the peak intensity for typical ion lasers, but below that for pulsed lasers.

Nonetheless, accurate PLIF measurements can be made with excitation intensities above the weak excitation limit, so long as the system is optically thin (Melton and Lipp 2003; Shan et al. 2004). In this scenario, dye absorption does not produce variations in I, and the non-linear relationship between F and I becomes moot. Furthermore, linearity between F and C has been demonstrated to persist at high intensities ($I > I_{sat}$) for fluorescein (Karasso and Mungal 1997), rhodamine WT (Melton and Lipp 2003), and rhodamine 6G (Shan et al. 2004), facilitating system calibration. An important caveat is that two studies (Karasso and Mungal 1997; Pan and Meng 2001) show seemingly anomalous behavior when fluorescein is used with Nd:YAG lasers. Both studies measured an initial *increase* in fluorescence along the direction of laser propagation in a uniform concentration of fluorescein, followed by the expected decay. Further studies are needed to determine if this is due to deviations from the Beer–Lambert law (determined by directly measuring the laser intensity attenuation) and/or due to fluorescence saturation effects.

3.2 Fluorescent dyes

Primary factors that govern the suitability of a particular dye include an absorption spectrum that is compatible with available laser excitation, a large separation between absorption and emission spectra, and high quantum efficiency to maximize signal strength (Arcoumanis et al. 1990). Other considerations include the degree of fluorescence sensitivity to temperature and pH (Smart and Laidlaw 1977; Walker 1987; Coppeta and Rogers 1998), susceptibility to photobleaching by the excitation source (Crimaldi 1997; Wang and Fiedler 2000a; Larsen and Crimaldi 2006), and fluorescence linearity with concentration (Karasso and Mungal 1997; Melton and Lipp 2003; Shan et al. 2004).

For aqueous PLIF applications, the choice of fluorescent dye is limited to those that are at least slightly water soluble. The most common aqueous PLIF dyes are fluorescein and two rhodamine dyes (rhodamine 6G, rhodamine B). These three xanthene-class dyes are all water soluble, with quantum efficiencies greater than 95%. Many dye properties reported in the literature (including those for water-soluble dyes) were measured using ethanol as the dye solvent. Since properties such as absorption and emission spectra, absorption coefficients, and diffusivities depend on the choice of solvent (Ware et al. 1983), ethanol-derived property values may be inaccurate for aqueous solutions. Table 1 summarizes basic measured parameters for the three most common PLIF dyes in aqueous solutions. Fluorescein (a.k.a. Uranine, disodium salt) is the most commonly used dye. Fluorescein has peak absorption near 490 nm (enabling efficient excitation with the 488 nm line of an argon-ion laser), peak emission near 510 nm, and has relatively low sensitivity to temperature changes (Walker 1987; Coppeta and Rogers 1998). However, the absorption spectra of fluorescein is strongly pH-dependent, such that absorption (and hence fluorescence) becomes negligible for pH < 4 (Walker 1987). This pH sensitivity can be exploited for mixing studies, as reviewed later. Fluorescein is known to be susceptible to photobleaching (Saylor 1995; Crimaldi 1997), but this problem has been shown to be minimal for typical PLIF applications (Larsen and Crimaldi 2006).

Rhodamine 6G (a.k.a. Rhodamine 590) has peak absorption near 525 nm (enabling excitation with either the 514.5 nm line of an argon-ion laser or the 532 nm line from a Nd:YAG), and peak emission near 560 nm. The dye is highly resistant to photobleaching (Crimaldi 1997; Larsen and Crimaldi 2006). Temperature and pH dependence data for this dye are scarce.

Rhodamine B (a.k.a. Rhodamine 610) has a peak absorption near 555 nm, but the absorption spectrum is broad enough to permit excitation at either 514.5 or 532 nm. The fluorescence of Rhodamine B is sensitive to changes in temperature (Sakakibara et al. 1993; Lemoine

Table 1 Properties of three common fluorescent dyes commonly used for aqueous PLIF

Dye	λ_{abs} (nm)	λ_{em} (nm)	ε (cm M)$^{-1}$	D (cm^2/s)	Percentage per °C
Fluor.	490	515[a]	8.5E4[b] (488.0 nm)	5.1E-6[c]	−0.2[a]
Rh. 6G	525	555[d]	1.1E5[e] (514.5 nm)	1.2E-6[f]	
Rh. B	555	580[a]	8.6E4[a] (514.5 nm)	3.7E-6[c]	−1.8[g]

The table gives the peak absorption (λ_{abs}) and emission (λ_{em}) wavelengths, the absorption coefficient (ε, as measured at the wavelength given in parenthesis), the molecular diffusivity (D) at 20°C, and the fluorescence sensitivity to temperature measured as percent change in fluorescence per °C near 20°C

[a] Coppeta and Rogers (1998)

[b] Walker (1987)

[c] Rani et al. (2005)

[d] Penzkofer and Leupacher (1987)

[e] Ferrier et al. (1993)

[f] Axelrod et al. (1976); Walker (1987)

[g] Sakakibara et al. (1993)

et al. 1999; Unger and Muzzio 1999; Bruchhausen et al. 2005), but relatively insensitive to changes in pH. The temperature sensitivity can be exploited to use PLIF for temperature measurements, as reviewed later. Rhodamine B may have acute and chronic health effects in case of skin or eye contact, or inhalation or ingestion, and is considered to be by far the most toxic of the xanthene dyes (Smart and Laidlaw 1977). Rhodamine WT has similar spectral characteristics to Rhodamine B, has been used in a few PLIF experiments (e.g., Monismith et al. 1990; Melton and Lipp 2003; Wadley and Dawson 2005), and might be a safer alternative to Rhodamine B for many experiments.

Synthetic substitutes for common xanthene dyes have become available in recent years and have been occasionally used in aqueous PLIF experiments (e.g., Stohr et al. 2003). These water-soluble substitutes are brighter, less susceptible to photobleaching, and less pH-sensitive than the dyes they replace (Panchuk-Voloshina et al. 1999), but they are also more expensive. Current examples include the Alexa Fluor dyes from Molecular Probes (Invitrogen Corporation), Hilyte Fluor dyes from AnaSpec, and DyLight dyes from Pierce (Thermo Fischer Scientific).

3.3 Sheet optics

Sheet-forming optics are used to transform the laser beam into a sheet within the flow. The sheet optics typically reside just outside the flow apparatus, and the beam is delivered there via either mirrors or a fiber optic cable (Koga et al. 1987). The most common approach (Fig. 2a) for forming a PLIF laser sheet uses a cylindrical lens (e.g., Dimotakis et al. 1983; Ferrier et al. 1993). A second approach (Fig. 2b) uses a rotating mirror to rapidly scan the incident beam one or more times across the image area. In some cases (e.g., Barrett and Van Atta 1991; Stapountzis et al. 1992), a rotating polygon with mirrors on each facet is rapidly rotated such that each facet produces a single laser scan. Alternatively, a single mirror is actuated by a galvanometer (e.g., Catrakis and Dimotakis 1996; Crimaldi and Koseff 2001), which can be controlled by an analog voltage signal from a signal generator or a computer.

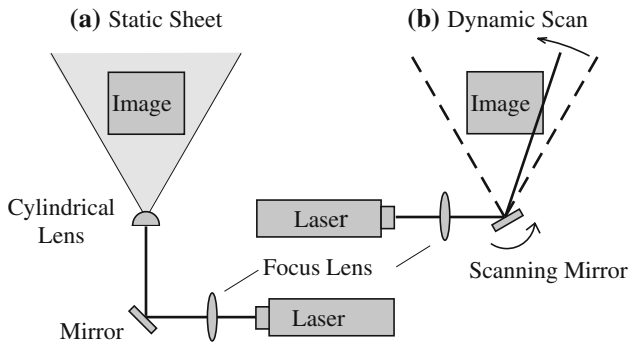

Fig. 2 Schematic for the optics used for the two most common laser sheet types. Details of the focus lens are shown in Fig. 4

Moving fluorescent features imaged over a finite duration will necessarily experience distortion in the resulting PLIF image. The magnitude of the distortion depends on the ratio of the image integration time to a relevant advective timescale. The character of the distortion depends on whether the image was made using a cylindrical lens ("static sheet") or a scanning mirror ("dynamic scan"). Numerical simulations of simplified scenarios are useful to illustrate the two types of distortion (Fig. 3). The middle panel shows a set of five idealized filaments, each in the shape of a + . Advection with speed u is from left to right, causing the filaments to advect a distance $\delta = ut_{\mathrm{exp}}$ to the right during the PLIF image exposure time t_{exp}. The top panel shows a simulation of the resulting PLIF image using a static sheet. The image exhibits blurring of features in the advective direction. This is a local distortion that can be minimized by requiring that

$$\Re_1 = \frac{\delta}{\lambda_s} \ll 1 \tag{16}$$

where λ_s is a length scale for local scalar filaments or features. For the simulation shown in Fig. 3, $\Re_1 = 4$ if λ_s is

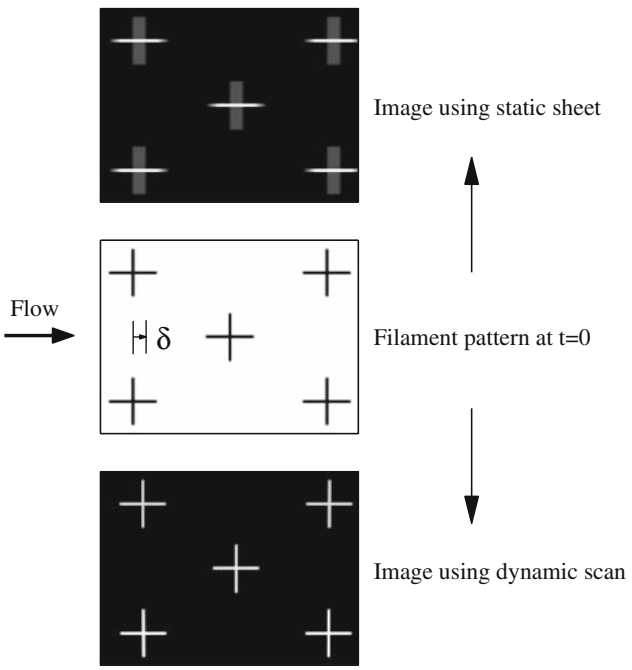

Fig. 3 Numerical simulations of distortion resulting from the two different types of laser sheets shown in Fig. 2. Advection is from left to right. The *middle panel* shows the initial position of five idealized filaments (each in the shape of a +). During the PLIF exposure interval t_{exp}, the filaments advect a distance δ to the right. The *upper* and *lower panels* show the PLIF image resulting from a static sheet and a dynamic scan, respectively. The total exposure time and fluorescence is identical in each case, but the nature of the advective distortions is different, as discussed in the text

chosen as the filament width (i.e., the width of the lines that form the + , which are strongly blurred), and $\Re_1 = 0.3$ if λ_s is chosen as the feature scale (i.e., the size of the + , which is reasonably well imaged). Note, too, that the distances between features on opposite sides of the image are accurately represented. By way of contrast, a simulation of the PLIF image obtained with a dynamic scan is shown in the lower panel, using the same advection velocity and image integration time as in the static case. Because small-scale features are exposed only for the short duration during which the high intensity laser beam passes over the corresponding pixels, the local resolution is extremely sharp, with no discernible blurring. However, the image exhibits distortion of the spatial relationships between features separated in the advective direction. The horizontal distance between the + features is slightly reduced relative to their actual separation shown in the middle panel. The distance is reduced because the simulated dynamic scan is from right to left (against the advection). Had this been reversed, the distances would increase by an equal amount. This is a global distortion that can be minimized by requiring that

$$\Re_2 = \frac{\delta}{L} \ll 1 \tag{17}$$

where L is the length of the imaged area in the advective direction. For the simulation Fig. 3, $\Re_2 = 0.05$, consistent with the small observed global distortion. The $\Re_2$ inequality is typically much easier to satisfy relative to the $\Re_1$ inequality, which confers an advantage to the dynamic scan method when using CW lasers, especially if one is interested in small-scale behavior.

Since the out-of-plane resolution of the PLIF system is determined by the thickness of the laser sheet, it is often desirable to focus the laser beam (Fig. 4). A collimated laser beam with radius (to the e^{-2} intensity contour) w_L passing through a lens with focal length f has a radius $w(z)$ given by

$$w(z) = w_0\left[1 + \left(\frac{\lambda z M^2}{\pi {w_0}^2}\right)^2\right]^{1/2} \tag{18}$$

where z is the distance from the focal point, λ is the laser wavelength, w_0 is the minimum beam radius at $z = 0$, and

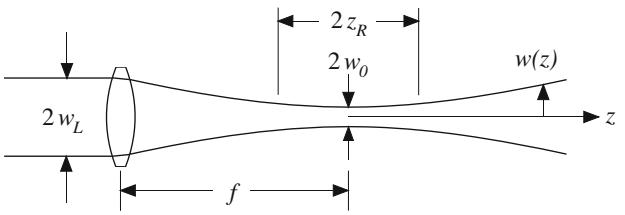

Fig. 4 Gaussian beam focus geometry. Adapted from Deusch and Dracos (2001)

M^2 is a beam quality parameter, where $M^2 = 1$ for an ideal Gaussian beam in TEM00 mode. Ion lasers typically operate in the range $1.1 < M^2 < 1.7$, but high energy multimode lasers can have $M^2 > 10$. The beam diameter or "spot size" at $z = 0$ is

$$2w_0 = 2M^2\frac{\lambda f}{\pi w_L} \tag{19}$$

Using a beam expander to increase w_L decreases w_0 for a given focal length lens. The working length over which the beam remains reasonably constant is called the Raleigh length, defined as

$$2z_R = 2\frac{\pi {w_o}^2}{\lambda} \tag{20}$$

such that $w(z_R) = \sqrt{2}w_0$. Focus lens configurations for laser sheets are shown in Fig. 2. If a beam expander is also used, it is placed between the laser and the focus lens.

It should be noted that Eqs. 18–20 represent best-case focus scenarios that are often not realized in typical laboratory settings. For this reason, it is often desirable to directly measure the sheet thickness by imaging the focussed beam as it passes through the test section.

3.4 Cameras

Traditional film cameras were used in the earliest PLIF experiments, with the resulting photographs used either in a qualitative sense (Dimotakis et al. 1983; Koochesfahani et al. 1985), or digitized for quantitative analysis (Shlien 1988). By the early 1990s, however, CCD digital cameras were used for PLIF (e.g., Prasad and Sreenivasan 1990; Koochesfahani and Mackinnon 1991), and their use has subsequently become the norm for acquiring fluorescence data. Since fluorescence occurs in a narrow wavelength band, color cameras are typically not used in favor of the higher performance available in grayscale cameras.

The choice of a digital camera for a particular PLIF application is typically a trade-off between maximizing pixel count, bit-depth, and framing rate. The pixel count influences spatial resolution, and ranges from as low as 256 × 256 (e.g., Van Vliet et al. 2004) to as high as 1,376 × 1,024 (e.g., Bruchhausen et al. 2005; Matsumoto et al. 2005). The bit-depth determines intensity resolution; a digital camera with a bit-depth N can resolve a maximum of 2^N discrete grayscales. The majority of PLIF experiments use 8-bit cameras, but 10-bit (Diez et al. 2005) and 12-bit (e.g., Pan and Meng 2001; Matsumoto et al. 2005) cameras are used to capture more of the dynamic range of concentrations in a system. The framing rate sets the maximum rate at which images can be acquired (this rate may also be limited by the system used to store the

images). For high-speed PLIF applications, framing rates as high as 955 frames per second have been used (Van Vliet et al. 2004). A final consideration is the spectral sensitivity of the camera. The sensitivity of the CCD chip at the wavelength of the fluorescence influences the required exposure time for a given image.

The use of a specialty flat-field lens is often warranted for PLIF imaging (e.g., Crimaldi and Koseff 2001). Flat-field lenses are designed to focus on planar surfaces, even with a small depth of field (large lens aperture). Most ordinary lenses have a spherical field characteristic, whereby the location of focussed objects is on a radial arc from the sensor. Since laser light sheets are flat, and limited fluorescence signal often dictates the use of large apertures, a flat-field lens can promote focal sharpness across the entire image.

A narrow-band optical filter is typically placed in front of the camera lens to allow only the fluorescence wavelengths to be imaged. Since many CCD sensors are sensitive to UV radiation, these filters often include blocking into the UV band.

4 Image processing

Raw PLIF images captured by the camera need to be post-processed for error correction and calibration. A robust form of image processing involves the use of a background image of a uniform, known concentration to implicitly determine the constants $\alpha(i, j)$ defined in Eq. 12. The background concentration is also present during the actual experiment. The description herein of this technique is an extension of processing algorithms used by Koochesfahani and Dimotakis (1985), Prasad and Sreenivasan (1990), Catrakis and Dimotakis (1996), Borg et al. (2001), Crimaldi and Koseff (2001), and others.

The dye concentrations present in the nth image are decomposed as $C_n(i, j) = c_n(i, j) + b_n$, where b_n is the uniform background concentration present at the time the image was taken, and $c_n(i, j)$ is the concentration structure above the background (the desired result). The attenuation coefficient given by Eq. 9 then becomes $a(r, \theta) = a_c(r, \theta)\, a_b(r)$, where a_c and a_b are the local attenuations due to c_n and b_n, respectively. The fluorescence intensity (Eq. 11) in an image of only the uniform background is

$$B_n(i,j) = \alpha(i,j) a_b(r) b_n + D(i,j) \tag{21}$$

where $D(i, j)$ is the dark-response of the camera. The dark response can be quantified as the average of a number of images acquired with the lens cap covered, with the camera at typical operating temperatures. When other dye in addition to the background is present, the recorded fluorescence intensity in the nth image is

$$I_n(i,j) = \alpha(i,j) a_c(r,\theta) a_b(r) [c_n(i,j) + b_n] + D(i,j) \tag{22}$$

Equations 21 and 22 can be combined to give an expression for $c_n(i,j)$ that does not include any explicit reference to $\alpha(i,j)$

$$c_n(i,j) = \frac{b_n}{a_c(r,\theta)} \frac{I_n(i,j) - [a_c(r)(B_n(i,j) - D(i,j)) + D(i,j)]}{B_n(i,j) - D(i,j)} \tag{23}$$

In the common scenario where $I_n \gg (B_n - D)$, Eq. 23 is accurately approximated by (noting that $a_c(r)$ is order unity for modest attenuations)

$$c_n(i,j) \approx \frac{b_n}{a_c(r,\theta)} \frac{I_n(i,j) - B_n(i,j)}{B_n(i,j) - D(i,j)} \tag{24}$$

This approximation decouples the attenuation correction $a_c(r)$ from the rest of the image processing algorithm, permiting a step-wise correction scheme. First, the raw images are flat-fielded through the $(I_n - B_n)/(B_n - D)$ calculation. Second, the images are scaled to dimensional units through multiplication by b_n. Finally, the resulting images are corrected for attenuation via division by $a_c(r, \theta)$, where $a_c(r, \theta)$ is calculated from the dimensional, flat-fielded images using Eq. 9.

The requirement for Eq. 24 that $I_n \gg (B_n - D)$ can be in conflict with the desire to have $B_n - D$ itself sufficiently large to avoid discretization and noise errors in the background image. This conflict is most easily resolved through the use of a camera with a large bit depth. For example, using a 12-bit camera (gray-scale values from 0 to 4,095) with typical pixel values of $D = 50$, $B_n = 200$, $I_n = 2{,}000$, and $a(r, \theta) = 0.9$ the approximation error in Eq. 24 is less than 1%.

In Eq. 24, the dye concentration in the background image b_n must be known a priori. This can be accomplished either with a fluorometric measurement, or by an explicit dose calculation. In most cases, the background concentration will be changing over time due to addition of additional dye during the experiment. In this case, multiple background images are usually used, and image interpolation in time can be used for intermediate images (Crimaldi and Koseff 2001). The calibration from pixel intensity to dimensional concentration can also be done with a calibration curve generated from multiple known concentrations mixed in the test apparatus (Karasso and Mungal 1996; Unger and Muzzio 1999).

In lieu of using the background-image correction technique described by Eq. 24, it is possible to explicitly correct for some errors introduced by the light sheet and imaging optics. A lens calibration image can be used to correct for lens vignette (Ferrier et al. 1993), and geometrical considerations can be used to calculate and correct for light sheet intensity variations (Diez et al. 2005). For a

radial laser sheet generated with a mirror with constant scan rate (see Fig. 1), the non-dimensional cartesian intensity of the resulting sheet is given by

$$I^*(x^*, y^*) = \left(x^{*2} + y^{*2}\right)^{-\frac{1}{2}} \tag{25}$$

where x and y are normalized by y_0, the value of y at the bottom edge of the image, and I^* is the intensity distribution normalized by the reference intensity $I(x^* = 0, y^* = 1)$. The resulting sheet intensity along with horizontal and vertical profiles is shown in Fig. 5. Laser sheets formed with mirrors rotating at non-uniform rates will produce different intensity profiles. This approach has been used to mitigate spatial variations in concentrations (Webster et al. 2003), and to eliminate the horizontal intensity variation seen in Fig. 5 (Crimaldi and Koseff 2001).

Table 2 summarizes common sources of error along with possible corrections and/or mitigations. In all cases, Eq. 24 corrects only errors that are invariant in time, or whose variation (e.g., linear) is known between any pair of background images. Additional procedures may be used for errors not corrected by Eq. 24. In particular, a correction for shot-to-shot variations in laser power variation when using pulsed lasers is typically necessary. This is typically done either by picking off a small portion of the laser power and measuring it with a power meter for each image (Coolen et al. 1999), passing the beam through a small cuvette with known concentration and measuring the fluorescence (Shan et al. 2004), or by making use of a constant concentration visible in each image (Guillard et al. 1998).

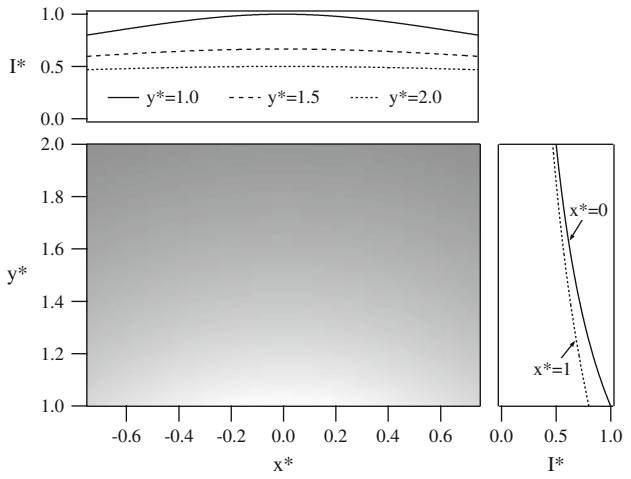

Fig. 5 Synthetic image of the non-dimensional intensity distribution of a laser sheet formed by a mirror rotating at constant angular rate (Eq. 25). The mirror is located at (0, 0). Also shown are *horizontal* and *vertical* profiles of the intensity

Table 2 Summary of error sources with corrections and/or mitigations

Category	Source	Correction	
		Equation 24	Other
Dye	Fluorescence from background dye	✔	
	Fluorescence sensitivity to pH and temperature	✔	
	Fluorescence saturation (strong excitation)	✔[a]	
	Photobleaching		✔[b]
Excitation	Spatial variation in light sheet (optics, etc.)	✔	
	Laser attenuation due to background dye	✔	
	Laser attenuation due to instantaneous dye		✔[c]
	Shot-to-shot laser power variation		✔[d]
Optics	Refraction through walls or interfaces		✔[e]
	Lens vignette	✔	
CCD	Pixel-to-pixel offsets (dark response)	✔	
	Pixel-to-pixel gain variations	✔	

Table adapted from Crimaldi and Koseff (2001)

[a] Only for optically thin solutions; see Sect. 3.1

[b] Not significant for most PLIF applications (Larsen and Crimaldi 2006)

[c] Corrected via Eq. 14, or mitigated with low dye concentration and/or short pathlengths

[d] Typically mitigated through closed-loop operation of CW lasers; see text for other corrections

[e] Explicit correction via grid image (Ferrier et al. 1993)

5 Applications

5.1 Scope of aqueous PLIF studies

LIF has been adapted for use with a wide range of flow types, with the principal requirement being that there is optical access to the measurement region for the laser sheet and fluorescence imaging. LIF studies have been done in open channels (Shiono and Feng 2003; Webster et al. 2003), pipes (Sakakibara et al. 1993; Pan and Meng 2001), microchannels (Matsumoto et al. 2005), stirred reactors (Houcine et al. 1996; Arratia and Muzzio 2004), rotating tanks (Horner-Devine 2006), and porous media (Rashidi et al. 1996; Stohr et al. 2003). The technique has been used to investigate scalar structure in boundary layers (Chen et al. 2007; Wagner et al. 2007), mixing layers (Koochesfahani et al. 1985; Koochesfahani and Mackinnon

1991; Karasso and Mungal 1996), stratified flows (Barrett and Van Atta 1991; Shy and Breidenthal 1991; Sakakibara et al. 1993; Nash et al. 1995; Atsavapranee and Gharib 1997; Daviero et al. 2001; Onishi and Komori 2006), internal waves (Troy and Koseff 2005a), gravity fronts (Parsons and Garcia 1998; Samothrakis and Cotel 2006), passive plumes (Crimaldi et al. 2002b; Webster et al. 2003), buoyant plumes (Johari 1992; Ai et al. 2006), jets (Dimotakis et al. 1983; Dahm and Dimotakis 1990; Bhat and Narasimha 1996; Catrakis and Dimotakis 1996; Webster et al. 2001; Westerweel et al. 2002), jets in cross-flows (Yoda and Fiedler 1996; Niederhaus et al. 1997; Davidson and Pun 1999), in vortices (Yu et al. 2007), and in biological flows (Monismith et al. 1990; Koehl et al. 2001; Crimaldi et al. 2002a; Mead et al. 2003).

The most general application of PLIF is for measurement of spatial and temporal scalar structure. PLIF images of instantaneous spatial structure can be obtained by ensuring that the image integration time is short compared to advective and straining timescales. Multiple images of instantaneous structure can be averaged to form images of concentration statistics (e.g., mean concentration, concentration variance).

Assuming the exposure timescale criteria are met (e.g., Eqs. 16 and 17), the spatial resolution of instantaneous PLIF images is determined by the area imaged by a single pixel and the sheet thickness, since all of the fluorescence information within the resulting voxel is averaged to a single value. The scale of the smallest concentrations η_B in a flow is (Batchelor 1959)

$$\eta_B = \eta_K Sc^{-1/2} \tag{26}$$

where $Sc = \nu/D$ and η_K is the Kolmogorov scale. The molecular diffusivity D for standard fluorescent dyes in water (Table 1) is order 10^{-6} cm^2/s, meaning that Sc is order 10^4. Thus, the smallest concentration scales in the flow are roughly 100 times smaller than the smallest scales of motion, and are often smaller than the spatial resolution of conventional PLIF configurations. Discussions of concentration scales in the context of PLIF can be found in Prasad and Sreenivasan (1990), Miller and Dimotakis (1991), Dahm et al. (1991), Koochesfahani and Mackinnon (1991), and Wang and Fiedler (2000b).

5.2 Extensions of the technique

The basic PLIF technique has been extended to yield measurements beyond concentration statistics. When LIF is used simultaneously with a velocimetry technique, the scalar and velocity fluctuations can be correlated to calculate scalar fluxes (Papanicolaou and List 1988). To this end, PLIF has been paired with laser-Doppler velocimetry (LDV) (Hannoun and List 1988; Onishi and Komori 2006), particle image velocimetry (PIV) (Simoens and Ayrault 1994; Law and Wang 2000), particle tracking velocimetry (PTV) (Webster et al. 2001; Cowen et al. 2001; Chang and Cowen 2002), and molecular tagging velocimetry (MTV) (Koochesfahani et al. 2000). Because fluorescent dye moves passively within a flow, correlation techniques have been used to extract the velocity field directly from PLIF concentration images (e.g., Dahm et al. 1992; Tokumaru and Dimotakis 1995; Su and Dahm 1996).

The sensitivity of fluorescence to an independent scalar (typically temperature or pH) can be exploited to quantify the concentration of the independent scalar. In the simplest case, the entire flow has a uniform concentration of temperature-sensitive dye, but a heterogeneous temperature field. Using the temperature sensitivity of Rhodamine B (see Table 1), temperature statistics have been measured in thermally stratified pipes (Sakakibara et al. 1993), buoyant jets and plumes (Nash et al. 1995; Sakakibara et al. 1997; Lemoine et al. 1999), and convection-driven cavities (Coolen et al. 1999). In a more complicated approach (Coppeta and Rogers 1998; Sakakibara and Adrian 1999; Hishida and Sakakibara, 2000; Moghaddas et al. 2002), a second dye that is relatively insensitive to the independent scalar is also added to the flow, and is used to establish the local intensity of the excitation source (which has typically been modified by absorption from the two dyes). A hybrid version of these two approaches exploits the different temperature sensitivities of two spectral bands of a single dye to measure temperatures with a correction for local laser intensity (Bruchhausen et al. 2005). In an unrelated multi-dye PLIF technique, Stohr et al. (2003) studied the porous-media flow of two immiscible liquid phases using separate dyes to track each phase.

PLIF is easily adapted to quantify densities in stratified flows by simply adding fluorescent dye to the working fluid in an amount that is proportional to its relative density. This approach has been used to study the inhibition of mixing in stably stratified turbulence (Barrett and Van Atta 1991), and to investigate structures in stratified plane mixing layers (Atsavapranee and Gharib 1997). In a particularly elegant set of PLIF experiments, breaking internal waves on a density interface were visualized (Troy and Koseff 2005a) and subjected to a quantitative stability analysis (Troy and Koseff 2005b). In the study, fluorescence intensities were calibrated to quantify local density and salinity (Fig. 6). When using PLIF in variable-density flows, index-of-refraction variations are typically mitigated with additional solutes (e.g., Hannoun and List 1988; Barrett and Van Atta 1991; Atsavapranee and Gharib 1997; Campbell et al. 2004; Daviero et al. 2001; Troy and Koseff 2005a).

An early and enduring extension to the PLIF technique enabled the quantification of mixing. First used by

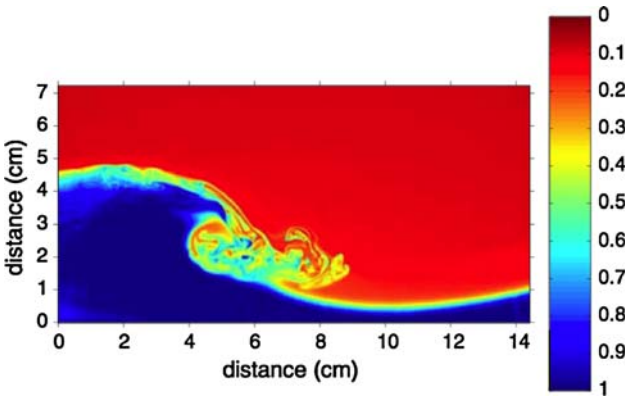

Fig. 6 PLIF image showing the structural details of a wave breaking at the interface of two-layer system. The layers have different salinities and dye concentrations, permitting concentration to be used as a surrogate for salinity. *Color* contours indicate normalized salinity. From Troy and Koseff (2005a)

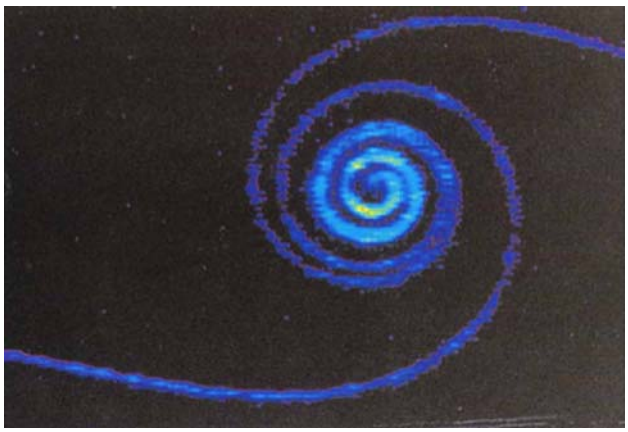

Fig. 7 PLIF image using the acid/base technique showing a laminar line vortex at the interface between two reactive fluid layers. Fluorescence occurs only where molecular diffusion mixes fluid from the two layers. The *false color scale* indicates reaction product for fast reactions. From Cetegen and Mohamad (1993)

Koochesfahani et al. (1985) to study reactions in an unstratified plane shear layer, the extension exploits the pH-sensitivity of fluorescein to selectively induce fluorescence in mixing regions. In the shear layer experiment, one fluid layer is dosed with fluorescein and buffered to a sufficiently low pH to suppress fluorescence. The second fluid layer has no dye, but is buffered to high pH. When mixing between the two layers occurs, the combination of resulting pH and dye concentration permits fluorescence with an intensity proportional to the product of a hypothetical fast chemical reaction between the fluids. Similar shear-layer experiments using the acid–base technique were later done in detail by Karasso and Mungal (1996). The acid–base PLIF technique has also been applied to the study of reactions in flows with buoyancy reversal (Shy and Breidenthal 1991; Johari 1992), in gravity fronts (Samothrakis and Cotel 2006), and to measure the free-surface mass boundary layer (Munsterer and Jahne 1998). An excellent example showing a chemically reacting laminar line vortex from Cetegen and Mohamad (1993) is shown in Fig. 7.

While the scope of the present review is limited to planar (2D) LIF, 3D LIF is implemented as an extension of PLIF, and thus warrants mention herein. In 3D LIF, a laser sheet is scanned perpendicular to the plane of the sheet, with images acquired in parallel (or approximately parallel) planes. The spatial resolution within the plane of the laser sheet is determined by the camera resolution and sheet thickness, and the resolution normal to the sheet is determined by the spacing of the scans. If multiple planes are sufficiently close and acquired sufficiently fast, frozen 3D scalar fields can be reconstructed. The two main challenges are being able to capture and store the images quickly enough, and having enough fluorescence exposure at the short image integration times. The first 3D LIF implementation in aqueous flows appears have to been done by Prasad and Sreenivasan (1990), who were able to acquire 8 parallel images in less than a millisecond. In other early studies, Dahm et al. (1991) and Yoda et al. (1994) used 3D LIF to investigate fine-scale 3D structure in turbulent jets. Since then, similar techniques have been used to investigate the three-dimensional scalar structure in impinging jets (Unger and Muzzio 1999), buoyant jets (Tian and Roberts 2003), tubular reactors (Van Vliet et al. 2004), and boundary layers (Delo et al. 2004). Three-dimensional temperature fields have been measured for natural convection from a heated plate (Sakakibara and Adrian 1999; Hishida and Sakakibara 2000), and for sheared, thermally stratified pipe flows (Hishida and Sakakibara 2000). A particularly elegant set of experiments was done by Deusch and Dracos (2001), whose volumetric scalar renderings from a free jet are shown in Fig. 8.

A relatively modern extension to the PLIF technique involves the use of "caged" dyes that are not fluorescent

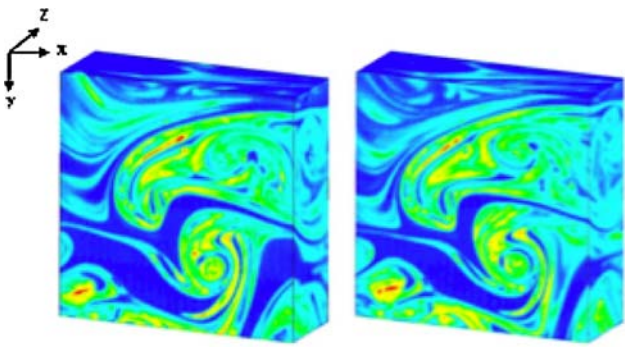

Fig. 8 Two consecutive 3D LIF volumes with dimensions $45 \times 45 \times 18$ mm^3 within a turbulent jet. From Deusch and Dracos (2001)

until they are permanently "uncaged" with a UV laser pulse. This permits small regions of the flow to be selectively rendered fluorescent and subsequently imaged using traditional PLIF with a second laser. The method has been used to track the evolution of small scalar features (Lempert et al. 1995), to measure velocities in a Poiseulle flow (Lempert et al. 1995) and to simultaneously measure concentrations and velocities in a turbulent shear layer (Koochesfahani et al. 2000).

6 Summary

The use of PLIF for non-invasive scalar measurements in aqueous flows has become widespread since its introduction over 25 years ago. Various refinements and correction procedures, combined with advances in digital imaging technology, have enabled the technique to evolve from a visualization tool to an accurate technique for quantifying scalar structure at high temporal and spatial resolution. PLIF has been employed in a wide range of experimental configurations, with the sole limitation being a requirement for optical access to the measurement region. Various extensions of the technique have been developed for measuring temperature, density, mixing rates, and scalar fluxes. PLIF is also easily extended for scalar measurements in three dimensions. Continuing advances in image acquisition, storage, and processing will likely result in volumetric laser-induced fluorescence (VLIF) replacing PLIF as the scalar measurement standard in aqueous flows.

Acknowledgments The author would like to thank Jennifer Morin for extensive help in researching this article. This work was supported by the National Science Foundation under CAREER Grant No. 0348855.

References

Ai JJ, Law AWK, Yu SCM (2006) On boussinesq and non-boussinesq starting forced plumes. J Fluid Mech 558:357–386

Arcoumanis C, McGuirk JJ, Palma J (1990) On the use of fluorescent dyes for concentration measurements in water flows. Exp Fluids 10(2–3):177–180

Arratia PE, Muzzio FJ (2004) Planar laser-induced fluorescence method for analysis of mixing in laminar flows. Ind Eng Chem Res 43(20):6557–6568

Atsavapranee P, Gharib M (1997) Structures in stratified plane mixing layers and the effects of cross-shear. J Fluid Mech 342:53–86

Axelrod D, Koppel DE, Schlessinger J, Elson E, Webb WW (1976) Mobility measurement by analysis of fluorescence photobleaching recovery kinetics. Biophys J 16(9):1055–1069

Barrett TK, Van Atta CW (1991) Experiments on the inhibition of mixing in stably stratified decaying turbulence using laser doppler anemometry and laser-induced fluorescence. Phys Fluids A Fluid Dyn 3(5):1321–1332

Batchelor G (1959) Small-scale variation of convected quantities like temperature in turbulent fluid. J Fluid Mech 5:113–133

Bhat GS, Narasimha R (1996) A volumetrically heated jet: large-eddy structure and entrainment characteristics. J Fluid Mech 325:303–330

Borg A, Bolinder J, Fuchs L (2001) Simultaneous velocity and concentration measurements in the near field of a turbulent low-pressure jet by digital particle image velocimetry-planar laser-induced fluorescence. Expe Fluids 31(2):140–152

Bruchhausen M, Guillard F, Lemoine F (2005) Instantaneous measurement of two-dimensional temperature distributions by means of two-color planar laser induced fluorescence (PLIF). Exp Fluids 38:123–131

Campbell JE, Coppom RW, Guilkey JE, Klewicki JC, McMurtry PA (2004) Time resolved concentration measurements in an axial flow mixer. J Fluids Eng Trans ASME 126(6):981–989

Catrakis HJ, Dimotakis PE (1996) Mixing in turbulent jets: scalar measures and isosurface geometry. J Fluid Mech 317:369–406

Cetegen BM, Mohamad N (1993) Experiments on liquid-mixing and reaction in a vortex. J Fluid Mech 249:391–414

Chang KA, Cowen EA (2002) Turbulent prandtl number in neutrally buoyant turbulent round jet. J Eng Mech ASCE 128(10):1082–1087

Chen DY, Chen CQ, Tang FE, Stansby P, Li M (2007) Boundary layer structure of oscillatory open-channel shallow flows over smooth and rough beds. Exp Fluids 42(5):719–736

Coolen MCJ, Kieft RN, Rindt CCM, van Steenhoven AA (1999) Application of 2-D LIF temperature measurements in water using a Nd:YAG laser. Exp Fluids 27(5):420–426

Coppeta J, Rogers C (1998) Dual emission laser induced fluorescence for direct planar scalar behavior measurements. Exp Fluids 25(1):1–15

Cowen EA, Chang KA, Liao Q (2001) A single-camera coupled PTV-LIF technique. Exp Fluids 31(1):63–73

Crimaldi JP (1997) The effect of photobleaching and velocity fluctuations on single-point LIF measurements. Exp Fluids 23(4):325–330

Crimaldi JP, Koseff JR (2001) High-resolution measurements of the spatial and temporal scalar structure of a turbulent plume. Exp Fluids 31(1):90–102

Crimaldi J, Koehl M, Koseff J (2002a) Effects of the resolution and kinematics of olfactory appendages on the interception of chemical signals in a turbulent odor plume. Environ Fluid Mech 2:35–63

Crimaldi JP, Wiley MB, Koseff JR (2002b) The relationship between mean and instantaneous structure in turbulent passive scalar plumes. J Turbul 3 (014):1–24

Dahm WJA, Dimotakis PE (1987) Measurements of entrainment and mixing in turbulent jets. AIAA J 25(9):1216–1223

Dahm WJA, Dimotakis PE (1990) Mixing at large schmidt number in the self-similar far field of turbulent jets. J Fluid Mech 217:299–330

Dahm WJA, Southerland KB, Buch KA (1991) Direct, high-resolution, 4-dimensional measurements of the fine scale structure of $Sc > 1$ molecular mixing in turbulent flows. Phys Fluids A Fluid Dyn 3(5):1115–1127

Dahm WJA, Su LK, Southerland KB (1992) A scalar imaging velocimetry technique for fully resolved 4-dimensional vector velocity-field measurements in turbulent flows. Phys Fluids A Fluid Dyn 4(10):2191–2206

Davidson MJ, Pun KL (1999) Weakly advected jets in cross-flow. J Hydraul Eng ASCE 125(1):47–58

Daviero GJ, Roberts PJW, Maile K (2001) Refractive index matching in large-scale stratified experiments. Exp Fluids 31(2):119–126

Delo CJ, Kelso RM, Smits AJ (2004) Three-dimensional structure of a low-reynolds-number turbulent boundary layer. J Fluid Mech 512:47–83

Deusch S, Dracos T (2001) Time resolved 3D passive scalar concentration-field imaging by laser induced fluorescence (LIF) in moving liquids. Meas Sci Technol 12(2):188–200

Dewey C (1976) Qualitative and quantitative flow field visualization utilizing laser-induced fluorescence. In: Proceedings of the AGARD conference of non-intrusive instrumentation in fluid flow research, AGARD-CP-193

Diez F, Bernal LP, Faeth GM (2005) PLIF and PIV measurements of the self-preserving structure of steady round buoyant turbulent plumes in crossflow. Int J Heat Fluid Flow 26:873–882

Dimotakis PE, Miakelye RC, Papantoniou DA (1983) Structure and dynamics of round turbulent jets. Phys Fluids 26(11):3185–3192

Ferrier AJ, Funk DR, Roberts PJW (1993) Application of optical techniques to the study of plumes in stratified fluids. Dyn Atmos Oceans 20(1–2):155–183

Guilkey JE, Gee KR, McMurtry PA, Klewicki JC (1996) Use of caged fluorescent dyes for the study of turbulent passive scalar mixing. Exp Fluids 21(4):237–242

Guillard F, Fritzon R, Revstedt J, Tragardh C, Alden M, Fuchs L (1998) Mixing in a confined turbulent impinging jet using planar laser-induced fluorescence. Exp Fluids 25(2):143–150

Hannoun IA, List EJ (1988) Turbulent mixing at a shear-free density interface. J Fluid Mech 189:211–234

Hansen L, Guilkey JE, McMurtry PA, Klewicki JC (2000) The use of photoactivatable fluorophores in the study of turbulent pipe mixing: effects of inlet geometry. Meas Sci Technol 11(9):1235–1250

Hishida K, Sakakibara J (2000) Combined planar laser-induced fluorescence-particle image velocimetry technique for velocity and temperature fields. Exp Fluids 29:S129–S140

Horner-Devine AR (2006) Velocity, density and transport measurements in rotating, stratified flows. Exp Fluids 41(4):559–571

Houcine I, Vivier H, Plasari E, David R, Villermaux J (1996) Planar laser induced fluorescence technique for measurements of concentration fields in continuous stirred tank reactors. Exp Fluids 22(2):95–102

Johari H (1992) Mixing in thermals with and without buoyancy reversal. J Atmos Sci 49(16):1412–1426

Karasso PS, Mungal MG (1996) Scalar mixing and reaction in plane liquid shear layers. J Fluid Mech 323:23–63

Karasso PS, Mungal MG (1997) PLIF measurements in aqueous flows using the Nd:YAG laser. Exp Fluids 23(5):382–387

Koehl MAR, Koseff JR, Crimaldi JP, McCay MG, Cooper T, Wiley MB, Moore PA (2001) Lobster sniffing: antennule design and hydrodynamic filtering of information in an odor plume. Science 294:1948–1951

Koga DJ, Abrahamson SD, Eaton JK (1987) Development of a portable laser sheet. Exp Fluids 5(3):215–216

Komori S, Nagata K, Kanzaki T, Murakami Y (1993) Measurements of mass flux in a turbulent liquid flow with a chemical-reaction. AICHE J 39(10):1611–1620

Koochesfahani MM, Dimotakis PE (1985) Laser-induced fluorescence measurements of mixed fluid concentration in a liquid plane shear-layer. AIAA J 23(11):1700–1707

Koochesfahani MM, Dimotakis PE (1986) Mixing and chemical-reactions in a turbulent liquid-mixing layer. J Fluid Mech 170:83–112

Koochesfahani MM, Mackinnon CG (1991) Influence of forcing on the composition of mixed fluid in a 2-stream shear-layer. Phys Fluids A Fluid Dyn 3(5):1135–1142

Koochesfahani MM, Dimotakis PE, Broadwell JE (1985) A 'flip' experiment in a chemically reacting turbulent mixing layer. AIAA J 23(8):1191–1194

Koochesfahani M, Cohn R, McKinnon C (2000) Simultaneous whole-field measurements of velocity and concentration fields using a combination of MTV and LIF. Meas Sci Technol 11(9):1289–1300

Larsen LG, Crimaldi JP (2006) The effect of photobleaching on PLIF. Exp Fluids 41(5):803–812

Law AWK, Wang HW (2000) Measurement of mixing processes with combined digital particle image velocimetry and planar laser induced fluorescence. Exp Therm Fluid Sci 22(3–4):213–229

Lemoine F, Wolff M, Lebouche M (1996) Simultaneous concentration and velocity measurements using combined laser-induced fluorescence and laser doppler velocimetry: application to turbulent transport. Exp Fluids 20(5):319–327

Lemoine F, Antoine Y, Wolff M, Lebouche M (1999) Simultaneous temperature and 2D velocity measurements in a turbulent heated jet using combined laser-induced fluorescence and LDA. Exp Fluids 26(4):315–323

Lempert WR, Magee K, Ronney P, Gee KR, Haugland RP (1995) Flow tagging velocimetry in incompressible-flow using photo-activated nonintrusive tracking of molecular-motion (PHANTOMM). Exp Fluids 18(4):249–257

Liu HT, Lin JT, Delisi DP, Robben FA (1977) Application of a fluorescence technique to dye-concentration measurements in a turbulent jet. In: Proceedings of the symposium on flow measurement in open channels and closed conduits. NBS Special Publication 484, pp 423–446

Matsumoto R, Zadeh HF, Ehrhard P (2005) Quantitative measurement of depth-averaged concentration fields in microchannels by means of a fluorescence intensity method. Exp Fluids 39(4):722–729

Mead K, Wiley M, Koehl M, Koseff J (2003) Fine-scale patterns of odor encounter by the antennules of mantis shrimp tracking turbulent plumes in wave-affected and unidirectional flow. J Exp Biol 206(1):181–193

Melton LA, Lipp CW (2003) Criteria for quantitative PLIF experiments using high-power lasers. Exp Fluids 35(4):310–316

Miller PL, Dimotakis PE (1991) Reynolds-number dependence of scalar fluctuations in a high schmidt number turbulent jet. Phys Fluids A Fluid Dyn 3(5):1156–1163

Moghaddas JS, Tragardh C, Kovacs T, Ostergren K (2002) A new method for measuring concentration of a fluorescent tracer in bubbly gas-liquid flows. Exp Fluids 32(6):728–729

Monismith SG, Koseff JR, Thompson JK, Oriordan CA, Nepf HM (1990) A study of model bivalve siphonal currents. Limnol Oceanogr 35(3):680–696

Munsterer T, Jahne B (1998) LIF measurements of concentration profiles in the aqueous mass boundary layer. Exp Fluids 25(3):190–196

Nash JD, Jirka GH, Chen D (1995) Large-scale planar laser-induced fluorescence in turbulent density-stratified flows. Exp Fluids 19(5):297–304

Niederhaus CE, Champagne FH, Jacobs JW (1997) Scalar transport in a swirling transverse jet. AIAA J 35(11):1697–1704

Onishi R, Komori S (2006) Thermally stratified liquid turbulence with a chemical reaction. AICHE J 52(2):456–468

Owen F (1976) Simultaneous laser measurement of instantaneous velocity and concentrations in turbulent mixing flows. In: Proceedings of the AGARD conference of non-intrusive instrumentation in fluid flow research, AGARD-CP-193

Pan G, Meng H (2001) Experimental study of turbulent mixing in a tee mixer using PIV and PLIF. AICHE J 47(12):2653–2665

Panchuk-Voloshina N, Haugland RP, BishopñStewart J, Bhalgat MK, Millard PJ, Mao F, Leung WY, Haugland RP (1999) Alexa dyes, a series of new fluorescent dyes that yield exceptionally bright, photostable conjugates. J Histochem Cytochem 47(9):1179–1188

Papanicolaou PN, List EJ (1988) Investigations of round vertical turbulent buoyant jets. J Fluid Mech 195:341–391

Papantoniou D, List EJ (1989) Large-scale structure in the far field of buoyant jets. J Fluid Mech 209:151–190

Parsons JD, Garcia MH (1998) Similarity of gravity current fronts. Phys Fluids 10(12):3209–3213

Patsayeva SV, Yuzhakov VI, Varlamov V (1999) Laser-induced fluorescence saturation for binary mixtures of organic luminophores. In: ICONO '98: laser spectroscopy and optical diagnostics: novel trends and applications in laser chemistry, biophysics, and biomedicine, SPIE, Moscow, Russia, vol 3732, pp 147–156

Penzkofer A, Leupacher W (1987) Fluorescence behavior of highly concentrated rhodamine 6g solutions. J Lumin 37(2):61–72

Prasad RR, Sreenivasan KR (1990) Quantitative 3-dimensional imaging and the structure of passive scalar fields in fully turbulent flows. J Fluid Mech 216:1–34

Rani SA, Pitts B, Stewart PS (2005) Rapid diffusion of fluorescent tracers into staphylococcus epidermidis biofilms visualized by time lapse microscopy. Antimicrob Agents Chemother 49(2):728–732

Rashidi M, Peurrung L, Tompson AFB, Kulp TJ (1996) Experimental analysis of pore-scale flow and transport in porous media. Adv Water Resour 19(3):163–180

Reynolds O (1883) An experimental investigation of the circumstances which determine whether the motion of water in parallel channels shall be direct or sinuous and of the law of resistance in parallel channels. Philos Trans R Soc 174:935–982

Sakakibara J, Adrian R (1999) Whole field measurement of temperature in water using two-color laser-indiced fluorescence. Exp Fluids 26:7–15

Sakakibara J, Hishida K, Maeda M (1993) Measurements of thermally stratified pipe-flow using image-processing techniques. Exp Fluids 16(2):82–96

Sakakibara J, Hishida K, Maeda M (1997) Vortex structure and heat transfer in the stagnation region of an impinging plane jet (simultaneous measurements of velocity and temperature fields by digital particle image velocimetry and laser-induced fluorescence). Int J Heat Mass Transfer 40(13):3163–3176

Samothrakis P, Cotel AJ (2006) Propagation of a gravity current in a two-layer stratified environment. J Geophys Res Oceans 111(C1):1–17

Saylor J (1995) Photobleaching of disodium fluorescein in water. Exp Fluids 18:445–447

Shan JW, Lang DB, Dimotakis PE (2004) Scalar concentration measurements in liquid-phase flows with pulsed lasers. Exp Fluids 36(2):268–273

Shiono K, Feng T (2003) Turbulence measurements of dye concentration and effects of secondary flow on distribution in open channel flows. J Hydraul Eng ASCE 129(5):373–384

Shlien DJ (1988) Instantaneous concentration field measurement technique from flow visualization photographs. Exp Fluids 6(8):541–546

Shy SS, Breidenthal RE (1991) Turbulent stratified interfaces. Phys Fluids A Fluid Dyn 3(5):1278–1285

Simoens S, Ayrault M (1994) Concentration flux measurements of a scalar quantity in turbulent flows. Exp Fluids 16(3-4):273–281

Smart P, Laidlaw I (1977) An evaluation of some fluorescent dyes for water tracing. Water Resour Res 13:15–33

Sreenivasan KR, Prasad RR (1989) New results on the fractal and multifractal structure of the large schmidt number passive scalars in fully turbulent flows. Physica D 38(1–3):322–329

Stapountzis H, Westerweel J, Bessem JM, Westendorp A, Nieuwstadt FTM (1992) Measurement of product concentration of 2 parallel reactive jets using digital image-processing. Appl Sci Res 49(3):245–259

Stohr M, Roth K, Jahne B (2003) Measurement of 3D pore-scale flow in index-matched porous media. Exp Fluids 35(2):159–166

Su LK, Dahm WJA (1996) Scalar imaging velocimetry measurements of the velocity gradient tensor field in turbulent flows. 2. Experimental results. Phys Fluids 8(7):1883–1906

Tian XD, Roberts PJW (2003) A 3D LIF system for turbulent buoyant jet flows. Exp Fluids 35(6):636–647

Tokumaru PT, Dimotakis PE (1995) Image correlation velocimetry. Exp Fluids 19(1):1–15

Troy C, Koseff JR (2005a) The generation and quantitative visualization of breaking internal waves. Exp Fluids 38:549–562

Troy CD, Koseff JR (2005b) The instability and breaking of long internal waves. J Fluid Mech 543:107–136

Unger DR, Muzzio FJ (1999) Laser-induced fluorescence technique for the quantification of mixing in impinging jets. AICHE J 45(12):2477–2486

Van Cruyningen I, Lozano A, Hanson RK (1990) Quantitative imaging of concentration by planar laser-induced fluorescence. Exp Fluids 10(1):41–49

Van Vliet E, Van Bergen SM, Derksen JJ, Portela LM, Van den Akker HEA (2004) Time-resolved, 3D, laser-induced fluorescence measurements of fine-structure passive scalar mixing in a tubular reactor. Exp Fluids 37(1):1–21

Wadley R, Dawson MK (2005) LIF measurements of blending in static mixers in the turbulent and transitional flow regimes. Chem Eng Sci 60(8–9):2469–2478

Wagner C, Kuhn S, von Rohr PR (2007) Scalar transport from a point source in flows over wavy walls. Exp Fluids 43(2–3):261–271

Walker D (1987) A fluorescence technique for measurement of concentration in mixing liquids. J Phys E Sci Instrum 20:217–224

Wang GR, Fiedler HE (2000a) On high spatial resolution scalar measurement with LIF—part 1: photobleaching and thermal blooming. Exp Fluids 29(3):257–264

Wang GR, Fiedler HE (2000b) On high spatial resolution scalar measurement with LIF—part 2: the noise characteristic. Exp Fluids 29(3):265–274

Ware B, Cyr D, Gorti S, Lanni F (1983) Electrophoretic and frictional properties of particles in complex media measured by laser light scattering and fluorescence photobleaching recovery. In: Dahneke BE (ed) Measurement of suspended particles by quasi-elastic light scattering. Wiley, New York, p 200

Webster DR, Roberts PJW, Ra'ad L (2001) Simultaneous DPTV/PLIF measurements of a turbulent jet. Exp Fluids 30(1):65–72

Webster DR, Rahman S, Dasi LP (2003) Laser-induced fluorescence measurements of a turbulent plume. J Eng Mech ASCE 129(10):1130–1137

Westerweel J, Hofmann T, Fukushima C, Hunt JCR (2002) The turbulent/non-turbulent interface at the outer boundary of a self-similar turbulent jet. Exp Fluids 33(6):873–878

Yoda M, Fiedler HE (1996) The round jet in a uniform counterflow: Flow visualization and mean concentration measurements. Exp Fluids 21(6):427–436

Yoda M, Hesselink L, Mungal MG (1994) Instantaneous 3-dimensional concentration measurements in the self-similar region of a round high-schmidt-number jet. J Fluid Mech 279:313–350

Yu SCM, Law AWK, Ai JJ (2007) Vortex formation process in gravity-driven starting jets. Exp Fluids 42(5):783–797